

## Technical Article

- Novel Magnetic Graphene Oxide Composite Material as a Solid-Phase Adsorbent for Uranium Removal

## Young Officer's FORUM

- IN-SITU Calibration System for Area Gamma Monitors and Autonomous Gamma Dose Loggers

## Young Researcher's FORUM

- Inter-droplet Force Between Magnetically Polarizable Pickering Oil-in-water Nanoemulsions Stabilized with  $\gamma$ -Al<sub>2</sub>O<sub>3</sub> Nanoparticles: Role of Electrostatic and Electric Dipolar Interactions

## News and Events

- Role of Nuclear and other Advanced Technologies for Climate Change Control
- Hindi Workshop
- Report on Transfer of IGCAR's Conductivity Meter Technology
- Women's Day Celebrations at IGCAR 2023

## Awards, Honours and Recognitions

## Bio-diversity @ DAE Campus, Kalpakkam



Director's Message

Dear Colleagues,

The fuel handling operation required for the 32nd campaign of FBTR was planned in two stages. The first stage of fuel handling operation to load two MK-1 fuel assemblies into the core, was completed. Reactor was started on 31st March to measure shutdown margin and operated at 25kWt to measure control rod worth. Commissioning of new 670 kW, 6.6 kV HT motor for Main Boiler Feed Pump (MBFP)-"A" was completed. An integrity test of MBFP motor-A for 100 hrs continuous operation was completed. All the mandatory surveillance checks including DG load test as per the planned schedule were carried out. 64th campaign for reprocessing of 105 GWd/t Burnup FBTR fuel in CORAL facility has been completed successfully.

The upgraded Online Nuclear Emergency Response System (ONERS-2) with provisions for radiological consequence assessments using Time-Dependent source Terms has been installed along with Numerical Weather Prediction & Dispersion Models on the High Performance Computing System at the Nuclear and Radiological Emergency Monitoring Cell, AERB Mumbai. The ONERS is used by NREMC-AERB for monitoring of emergency exercises and training purposes. The installation of C-Band Doppler Weather RADAR at Kalpakkam site in collaboration with ISTRAC has been completed. Endurance test and other commissioning works are in progress.

The transfer of Pulsating sensor-based conductivity meter technology developed in IGCAR to M/s. Lablink, Mumbai based industry on a non-exclusive basis was carried out as part of 'Atma Nirbhar Bharat' mission.

Women's day was celebrated from March 1-7, 2023, at IGCAR. Ministry of Women and Child Development had directed DAE to create awareness about the schemes developed by the government for the welfare of women. The celebrations included competitions and felicitating girl students who have excelled in studies, sports, and cultural events.

I appreciate the efforts of the editorial committee and the authors for their contributions to the newsletter.

[B. Venkatraman]  
Director IGCAR & GSO

## *Editor's Desk*

### *Dear Reader*

### *Greetings*

It is my pleasant privilege to forward the latest issue of IGC Newsletter ( Volume 136, April 2023, Issue 2). I thank my team for their timely inputs, cooperation, and support in bringing out this issue.

The technical article of this issue “Novel Magnetic Graphene Oxide Composite Material as a Solid-Phase Adsorbent for Uranium Removal” is by Dr. A. S. Suneesh and his colleagues from MCMFG, IGCAR.

Young Officer's Forum features an article on “IN-SITU Calibration System for Area Gamma Monitors and Autonomous Gamma Dose Loggers” by Ms. Athira B Varrier from SQRMG, IGCAR.

The article on “Inter-droplet Force Between Magnetically Polarizable Pickering Oil-in-water Nanoemulsions Stabilized with  $\gamma$ -Al<sub>2</sub>O<sub>3</sub> Nanoparticles: Role of Electrostatic and Electric Dipolar Interactions” by Ms. Ms. Manali Nandy from MMG, IGCAR is categorised as this issue's Young Researcher article.

In the back cover, we have Yellow-billed Babbler, a noisy and gregarious bird. It is commonly found in DAE township and IGCAR Campus.

The Editorial Committee would like to thank all the contributors. We look forward to receiving constructive suggestions from readers towards improving the IGC Newsletter content.

We express our deepest gratitude to Director IGCAR for his keen interest and guidance.

With best wishes and regards

S. Rajeswari

Chairman, Editorial Committee, IGC Newsletter and  
Head, Scientific Information Resource Division, IGCAR

## Novel Magnetic Graphene Oxide Composite Material as a Solid-Phase Adsorbent for Uranium Removal

The quest for more promising solid phase adsorbents, delivering superior selectivity of the target metal ions and economic viability, stirred the development of several advanced materials. Graphene, a Nobel prize-winning discovery, has not only kindled the interest of material scientists but also queered separation scientists in obtaining high selectivity solid phase adsorbents. Graphene, a monolayer allotrope of carbon, is a material with highly adaptable properties. Graphene constitutes a two-dimensional monolayer of  $sp^2$  hybridized carbon atoms with a honeycomb lattice structure. Despite the highly adaptable structural and surface properties, attention towards GO for the separation application has started quite recently. Provision for incorporating diverse ligands on its surface was the rationale for GO-based research on metal-ion separation on composite-GO adsorbents. Hummers' method or its modification is a well-recognized chemical procedure for preparing GOs from the commercially available graphite powder. It has also been known that oxidation of graphite matrix resulted in mono-layered graphene or graphitic oxide having fewer layers. The oxidation process also results in the formation of several functional groups on the matrix, viz. carboxyl, sulfonyl, hydroxyl and epoxy groups, is the basis behind GO being used in solid phase adsorption systems.

The advent of nuclear reactor programs is a consequence of the discovery of uranium, a naturally occurring fissile element. Besides, in pursuit of alternative energy sources to reduce emission of greenhouse gases, nuclear fission of uranium and its transmutation product, plutonium, forms the most promising source. Uranium finds its predominant use in nuclear reactors with a global consumption

of approximately 67,000 tU/yr, currently, despite its limited source in the earth's crust. Uranium minerals are widely obtained from igneous rocks, magmatic-hydrothermal families, phosphate rocks, etc. However, the uranium reserves available from the above sources would not sustain the estimated increase in energy demand (to  $\sim 150\%$  by 2050). It is also known that the seawater covering more than 70 % earth's surface by area could constitute uranium reserves of significant proportions, equating to over 4.5 billion tonnes. Even with ultra-low concentrations of uranium ( $\sim 3$  ng/mL), the total uranium content in seawater could amount to 1000 times of that present in conventional uranium minerals on the earth's crust. Health hazards of uranium are due to its radiotoxicity and heavy metal poisoning leading to nephrotoxic and carcinogenic effects in the human body. Other than its conventional sources (eg. uranium-mines), uranium recovery from sea water or other natural water bodies require sophisticated separation systems. Among the different separation methods studied, solid-phase separation of uranium is highly recommended in terms of economy, efficiency and the minimal quantity of secondary waste generation.

In IGCAR, we developed a GO-magnetite composite (MGO) adsorbent to separate uranium from the natural water bodies, such as seawater, uranium contaminated mine water, etc. Magnetite based adsorbents facilitate faster physical separation of the adsorbent phase from the aqueous phase. Contrast to the normal adsorbents, magnetite adsorbents are prepared with a view to achieve the faster separation under the influence of an external magnetic field. The lightweight properties limiting the scope of GO separation could be conveniently overcome by magnetic support ( $Fe_3O_4$ ). The MGO proposed in this report is unique among the previously reported ones in that, the adsorption of uranium on the MGO was facilitated by the  $-COOH$  functionalities on MGO itself, without the need of employing any other external ligand. In short, the present study will provide a preliminary understanding of how Hummers' oxidation can tune GO to create adsorption functionalities for uranium.

### Preparation of magnetic composite adsorbent

The GO was synthesized from commercially available graphite powder, using a modified Hummers' oxidation procedure. This involves oxidation of graphite using  $KMnO_4$ ,  $H_2SO_4$  and  $H_3PO_4$ , at  $50^\circ C$ . 2 mL of  $H_2O_2$  was added to the above reaction mixture to quench the reaction. The solid phase was separated from the aqueous solutions by filtration. After the filtration, the solid residue was washed four times with 2 M HCl and demineralized water (five times). The filtered GO particles were dried in air for 24 hours and in hot air oven (at  $60^\circ C$  under vacuum) for further 24 hours.

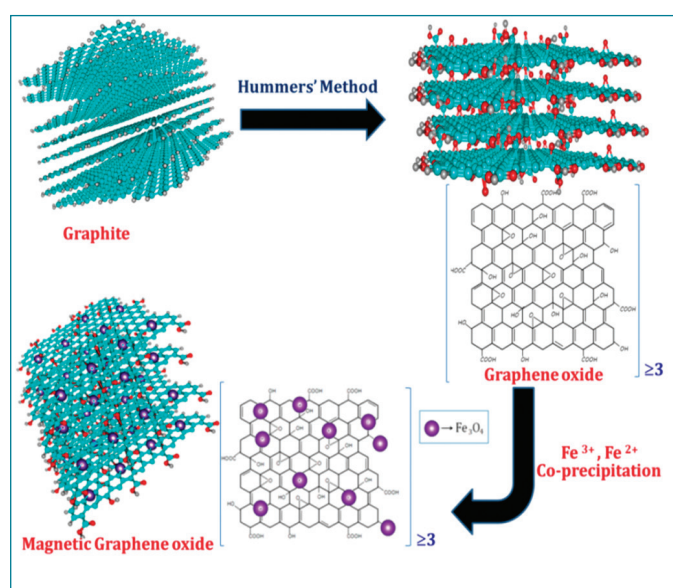


Figure 1: Scheme of synthesis of MGO from ultra-high pure graphite powder.

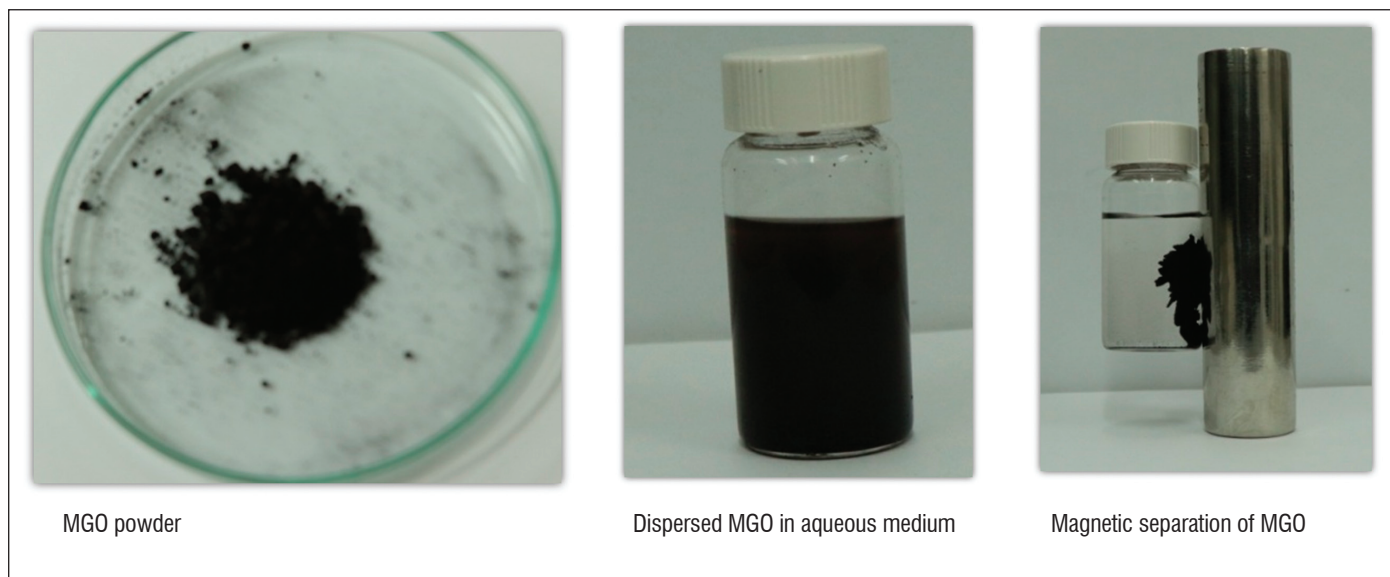


Figure 2. Photographs of various GO materials

The co-precipitation of  $\text{Fe}_3\text{O}_4$  is a standard procedure adopted, involving alkaline hydrolysis (using ammonia, 800 mL) of a mixture of  $\text{FeCl}_3$  (0.8 M, 10 g) and  $\text{FeSO}_4$  (0.4 M, 7.3 g) in millipore water (250 mL). Likewise, MGO was also prepared by a previously reported approach in which GO powder (Figure 2) was dispersed in the alkaline solution during the co-precipitation process. Excess ammonia was further added to maintain the alkalinity of the medium. The reaction was performed under argon atmosphere by refluxing at 85 °C for two hours. The MGO particles formed were separated from the mixture and washed several times with de-ionized water, isopropanol and acetone. The MGO particles were dried in air overnight before use (Figure 1). A permanent magnet (1 tesla, cylindrically shaped, of 100 mm length and 15 mm diameter) was used for the physical separation of magnetic particles from liquid

phase.

Figure 3 shows the SEM images of GO, magnetite  $\text{Fe}_3\text{O}_4$  particles and the MGO. Multiple 'layers' morphology of GO was observed from the SEM. Addition of magnetic  $\text{Fe}_3\text{O}_4$  has further enhanced the layer separation. The approximate thickness of the GO and MGO flakes is deduced to be 40 to 50 nm (obtained from the SEM images).

Raman spectra of GO,  $\text{Fe}_3\text{O}_4$ , and MGO are shown in traces 'a', 'b' and 'c' of Figure 4. Raman spectrum of GO shows peaks at  $\sim 1350\text{ cm}^{-1}$  and  $\sim 1580\text{ cm}^{-1}$  identified as defect (D) and graphitic (G) peaks, respectively and the latter is more intense than former in the synthesized GO. Additionally, there are three more bands in the region of  $2700\text{ cm}^{-1}$  to  $2900\text{ cm}^{-1}$  (not shown in the Figure). The G peak at  $1580\text{ cm}^{-1}$  is typical of C=C bonds in the carbon backbone of a few-layer GO structure. Raman spectroscopy shows a few layer

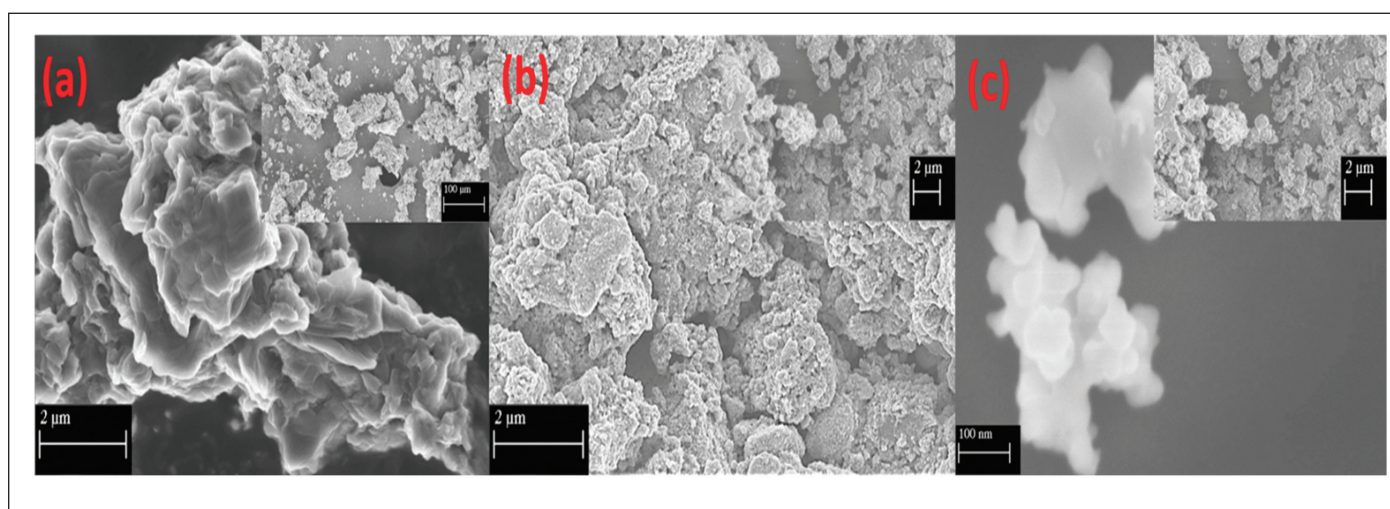


Figure 3. SEM images of GO (a),  $\text{Fe}_3\text{O}_4$  (b) and MGO(c). The inset is low magnification image showing the powdery nature of the bulk compound. The high resolution of MGO image shows the multilayered morphology of MGO.

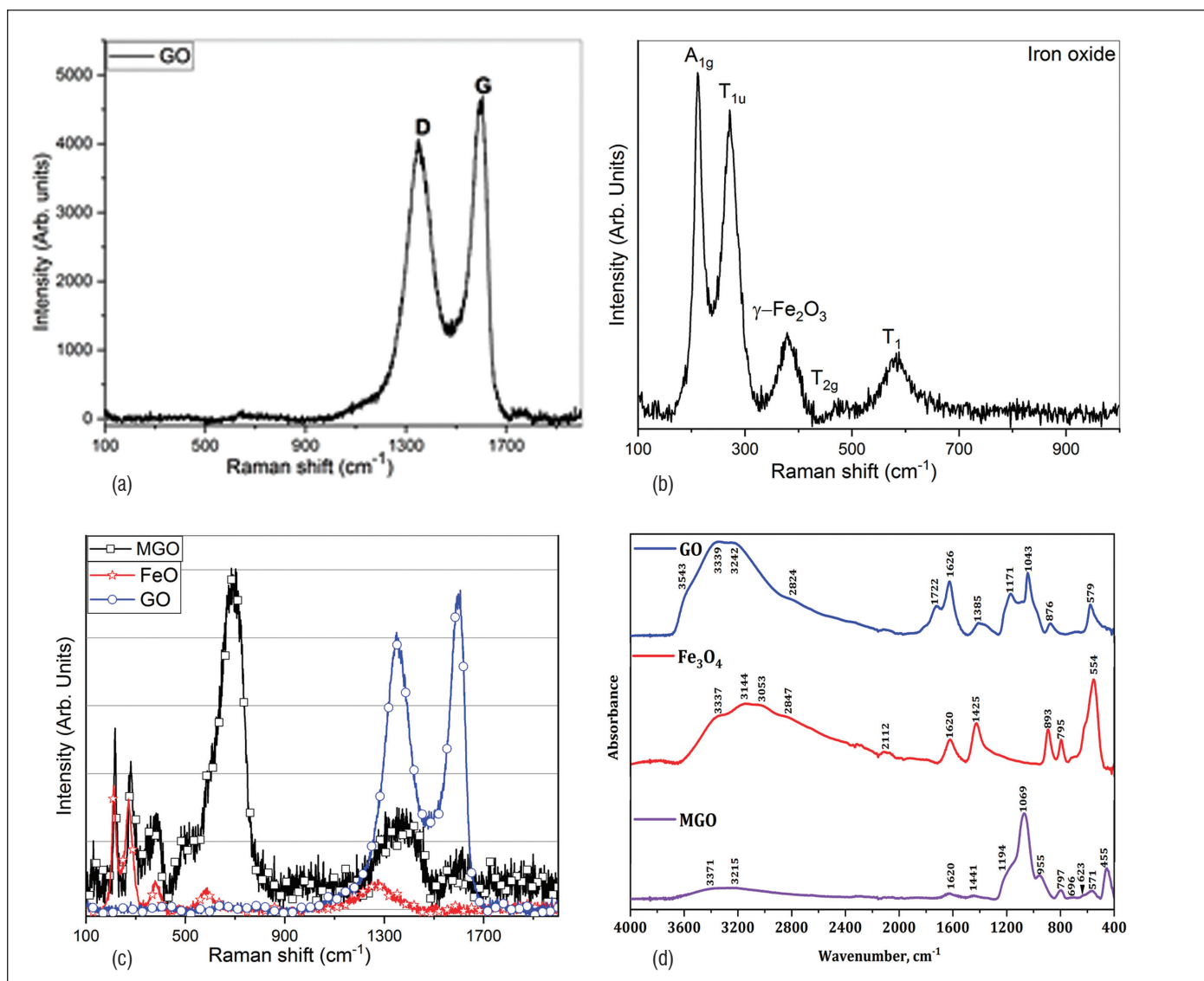


Figure 4. Raman spectra of (a) GO, (b) Fe<sub>3</sub>O<sub>4</sub> and (c) GO, Fe<sub>3</sub>O<sub>4</sub>, MGO superimposed. D and G peak indicate graphitic nature with defects in GO; d) FT-IR spectra of GO, Fe<sub>3</sub>O<sub>4</sub> and MGO.

Graphene based structure with large number of dangling bonds terminated with oxygen. Iron oxide shows peaks corresponding to magnetic iron oxide (Fe<sub>3</sub>O<sub>4</sub>) and maghemite ( $\gamma$ -phase). MGO shows peaks corresponding to Fe<sub>3</sub>O<sub>4</sub> and GO, however, a change in the intensity patterns of D and G peaks was observed for MGO in comparison to GO. The presence of the other phase likely influences the peak position and shape of MGO. Any peak shift to higher energy (cm<sup>-1</sup>) indicate hardening of the respective bonds and intensity reduction generally indicate annihilation of defects, however, we can't correlate the D peak in GO to that category because already it has very large number of defects and is in the 2nd stage of Ferrari amorphization trajectory where increase in defects actually cause reduction in ID/IG ratio. However, it is understood that chemical association of iron oxide with GO in MGO has indeed some useful effects which help fast separation of uranium.

The FT-IR spectrum of GO, Fe<sub>3</sub>O<sub>4</sub> and MGO are shown in trace

'd' of Figure 4. The multiple layered GO shows signature peaks at 1722/1626 cm<sup>-1</sup> that correspond to carbonyl (C=O) stretching associated with carboxylic acid groups. The peak at 1043 cm<sup>-1</sup> indicate the presence possibly of epoxy groups and the same can be due to S=O stretching frequency of sulphonic acid group. The sulphonic acid group can be introducing in GO as sulphuric acid is used as precursor in the synthesis of GO. The O-H stretching vibrations associated with hydroxyl group (of course sulphonic acid also) was observed as a broad band covering 3500-2800 cm<sup>-1</sup>. The feature at 876 cm<sup>-1</sup> corresponds to deformation vibrations of epoxides (C-O-C) and the band at 579 cm<sup>-1</sup> is due to stretching vibrations of pyran like ether (C-O). FT-IR spectra of MGO showed the signatures of both Fe<sub>3</sub>O<sub>4</sub> and GO, however with reduced intensity.

The XRD pattern of GO indicates the signature of a typical GO peak around 12°, which corresponds to (001) plane. It also showed the presence of graphite at 25° (corresponding to (002) plane).

Therefore, in combination with SEM images, XRD data also supported the formation of layered GO in Hummers' method of oxidation. The XRD pattern of MGO also shows peaks corresponding (311) planes of  $\text{Fe}_3\text{O}_4$  and (511) (002) planes of graphite.

### Adsorption behavior of uranium

The required amount of adsorbent (MGO) was dispersed in the aqueous phase containing uranium in a stoppered test tube. An orbital shaker was used to facilitate the agitation and thus the chemical exchange of uranium in the aqueous phase to MGO. The magnetic separation of MGO is demonstrated with a photograph in Figure 1, which indicates the faster separation of dispersed MGOs when a permanent magnet is placed close to the vial containing MGOs dispersed in the aqueous medium. Uranium concentrations of the aqueous phase before contact with the adsorbent and after agitation with the adsorbent were analyzed by UV-Visible spectrophotometry using the Arsenazo-III indicator. The absorbance corresponding to 540 nm, a characteristic absorbance peak of the uranium-Arsenazo III complex, was used to measure the uranium concentrations. Adsorption of uranium as a function of pH of the aqueous phase is shown in Figure 5 and an increase in uranium adsorption trend with the increase of pH is clearly demonstrated. Adsorption studies were also performed with nascent  $\text{Fe}_3\text{O}_4$  and GO. Uranium adsorption to

$\text{Fe}_3\text{O}_4$  was negligible. The poor adsorption tendency of  $\text{Fe}_3\text{O}_4$  to uranium adsorption is due to the absence of any chelating or cation exchange moiety. On the other hand, the high uranium adsorption on GO and MGO is attributed to the presence of cation exchange sulfonic and carboxylic acid groups. Since the sulfonic acid group is a strong cation exchange group, and therefore, the cation exchange mechanism is expected to be independent of the pH of the aqueous medium.

The carboxylic acid group being a weak cation exchange group is expected to exhibit an increase in uranium adsorption with increased pH. As observed experimentally, the adsorption efficiency was found to be < 10 % at pH=1 and < 40 % at pH=3 and an enhanced adsorption was clearly witnessed with MGO (or GO) at pH > 5. Figure 6 also shows that the uranium adsorption increases as a function of uranium concentration in the aqueous phase. The composition and concentration of uranium vary in samples from different oceans under the influence of salinity and other mineral ion compositions. Majority of the studies have reported that the average uranium concentration in seawater having 35 % salinity is approximately 3.3 ng/mL. Other than the alkali (K, Li, Na, Cs) and alkaline earth metals (Ca, Sr, Mg) and the uranium, transition elements (such as As, Fe, Zn, Mn, Mo, Ni, Pb, V) constitute a major portion of the cations present in ocean water. Therefore, in order

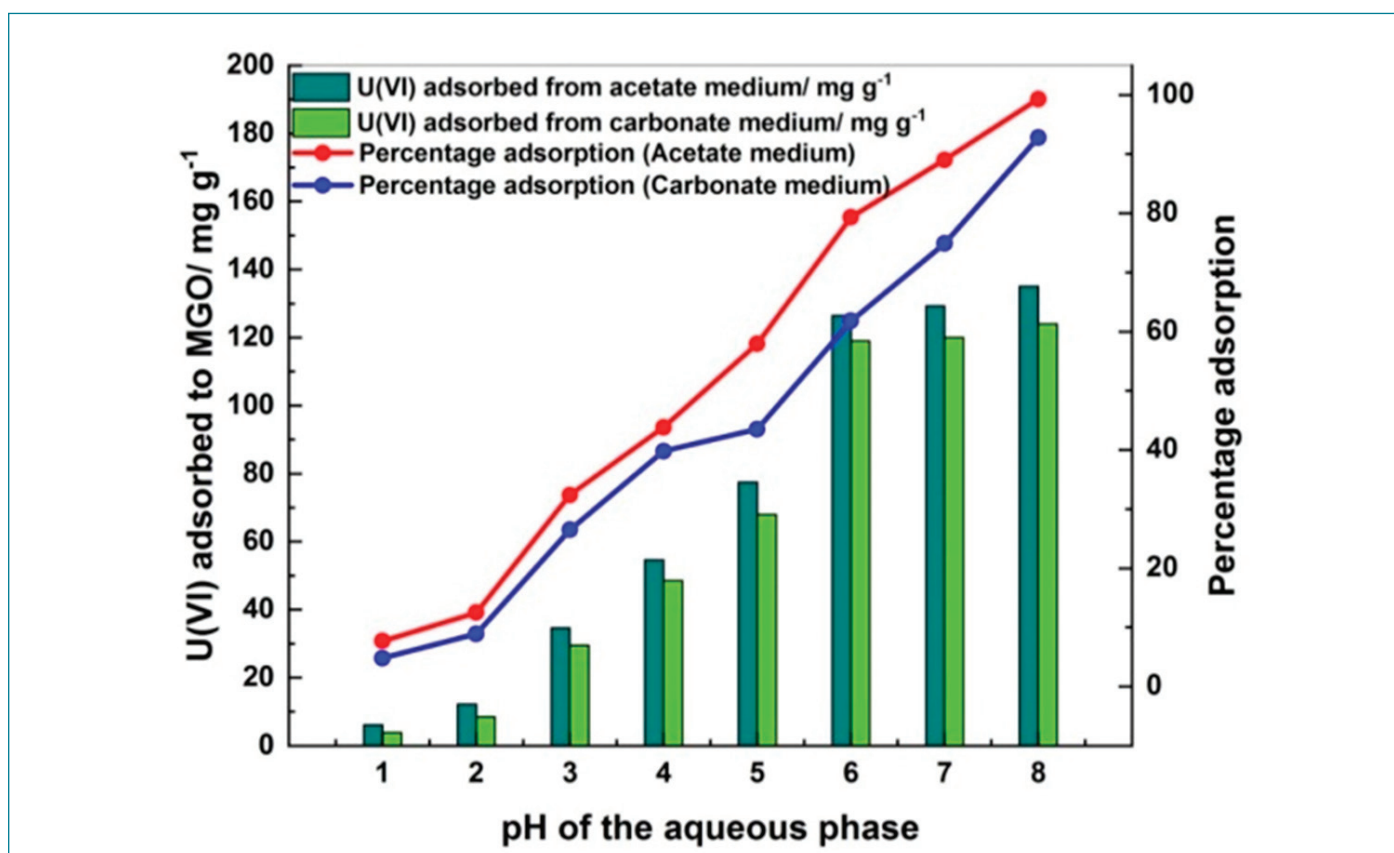


Figure 5. Adsorption of uranium to MGO. Adsorbent: 100 mg of MGO. Aqueous phase: 100 mg L<sup>-1</sup> of uranium present in sodium acetate or carbonate medium. For the acetate medium, required volume of 0.1 M sodium acetate and 0.1 M acetic acid buffer system was used at different pH values. For the carbonate medium, 0.1 M sodium carbonate at different pH values was used. T=298 K. Duration = 6 hours.

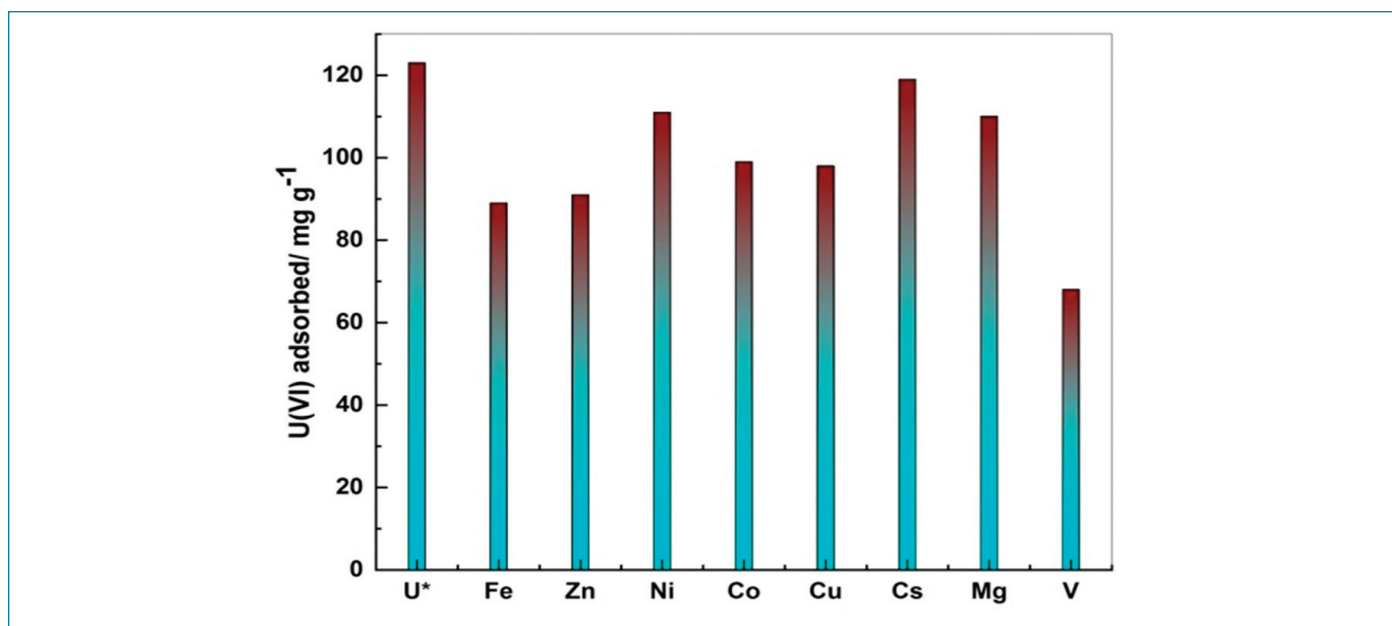


Figure 6. Adsorption of uranium to MGO in the presence of interfering (Fe, Zn, Ni, Co, Cu, Cs, Mg, V) ions. Adsorbent: 100 mg of MGO. Aqueous phase: 100 mg L<sup>-1</sup> uranium present in sodium acetate medium at pH 6. 200 mg L<sup>-1</sup> of the interfering ions is present as the chloride or nitrate salt. T=298 K. Duration = 6 hours. The asterisk on uranium represents adsorption of uranium in absence of other ions.

to understand the effect of the above interfering ions, the amount of uranium adsorbed onto MGO was determined in the presence of some of the interfering cations, such as Fe, V, Zn, Cu, Ni, Co, Cs and Mg and the results of which are shown in Figure 7. The amount of uranium in individual adsorption experiments involving uranium adsorption from the aqueous phase (acetate buffer medium at pH 6) contain 100  $\mu\text{g/mL}$  of uranium and 200  $\mu\text{g/mL}$  each of the interfering ions. Uranium adsorbed onto MGO without any interfering ions was 120 mg g<sup>-1</sup>. It can be seen from the Figure that, except during the presence of V, the highest reduction in uranium adsorption in the presence of other interfering ions was only 25 % in case of Fe. Reduction in adsorption of uranium in presence of other elements such as Zn, Cu, Ni, Co, Cs, and Mg was within 5 %. Uranium adsorption was reduced from 120 mg g<sup>-1</sup> to 65 mg g<sup>-1</sup> when 200  $\mu\text{g/mL}$  of V was present alongside 100  $\mu\text{g/mL}$  of U. This observation is very significant in terms of practical application MGO for uranium retrieval from sea water that motivated the analysis of underlying uranium chemistry further. Overall, efficiency of MGO in selectively separating uranium even in the presence of interfering cations is highly superior.

Performance of the adsorbent towards recycling-cum-reuse has also been investigated by repeated adsorption-cum-elution of metal ions to MGO phase. 0.1 M nitric acid was employed for the elution of uranium from MGO. Uranium adsorbed to MGO was quantitatively eluted in four to five cycles of contact with 0.1 M nitric acid. The elution efficiency was 99 % within four to five contacts of nitric acid with uranium-adsorbed-MGO. The recycled MGO also showed comparable-adsorption performance with that of neat (untreated) MGO, indicating that the adsorbent is suitable for repeated cycles

of operation. Therefore, based on recycling studies, the uranium adsorption performance of MGO is expected to be retained with at least 75 % efficiency even for 10 to 20 cycles of operations. Possible chemical degradation is insignificant for these materials. Moreover, quantitative removal of adsorbed uranium from the cation exchange-based functional group in MGO could also be a rationale for the improved recycling efficiency. It is worth mentioning that the uranium adsorption reported in the present study matches well with reports available in literature.

Overall, an advanced composite adsorbent based on graphene oxide, having magnetic separation feature, was synthesized and investigated for the separation of uranium from various aqueous solutions containing low concentrations of uranium as well as for the removal of uranium from natural water bodies such as sea water and mine water. The selectivity of MGO towards uranium was accomplished through carboxylic acid functional groups that is invoked during the synthesis of GO. Making GO magnetic aided in faster separation of uranium. The adsorption of uranium by MGO from acetate buffer medium was found to be strongly dependent on pH, and carbonate medium causes a minimal drop in uranium adsorption (less than 5 %). The role of various interfering ions in seawater was probed with the maximum adverse effect by V<sup>5+</sup>. Overall, the usefulness of the MGO as a solid phase adsorbent for efficient separation of uranium is firmly established through this study.

Reported by

Dr. A. S. Suneesh and Colleagues,  
ACSSS/FChD/FMCG/MC&MFCG

## Young Officer's Forum



Ms. Athira B Varrier joined in Radiological & Environmental Safety Division, IGCAR as Scientific officer-C after completing her training in Nuclear Reactor Physics from 64<sup>th</sup> batch of BARC training School in the year 2021. She is a topper of the college during her graduation in physics from Government Victoria College, Palakkad, Kerala in the year 2017. She is also ranked 1st in university during her post graduation in Physics from Central University of Kerala, Kasaragod. Currently she is working in the field of Radiation Metrology. She has presently designed an in-situ calibration system for carrying out calibration of Area Gamma Monitors and Autonomous Gamma Data Loggers. She is also involved in the process of setting up of a calibration facility for neutron detectors at RAMS, RESD.

## IN-SITU Calibration System for Area Gamma Monitors and Autonomous Gamma Dose Loggers

Area Gamma Monitors (AGM) and Autonomous Gamma Dose Loggers (AGDL) installed at various locations in DAE Complex, Kalpakkam is of paramount importance for ensuring radiological safety. These instruments are used for radiation monitoring of the working area with keen intent to reduce overexposure to radiation. It provides environmental radiation surveillance through continuous monitoring during normal operation. It helps us to detect immediately any increase in gamma dose rate specifically for area and process monitoring in nuclear facilities and alerts the working personnel in the event of a radiological emergency situation. Most of these AGM and AGDL use Geiger Muller (GM) tube as detector which displays the gamma dose in a particular area and provides audio and visual alarm indication with contact outputs whenever preset threshold levels are exceeded. As part of radiation protection, 33 AGMs and

28 AGDLs have been installed at various locations of DAE Complex, Kalpakkam.

It is very much essential to verify the functionality of these monitoring instruments for their appropriate usage. Periodic performance checking and calibration with standard source and testing of annunciation of alarms is necessary. Calibration is the quantitative determination, under a controlled set of standard test conditions, of the reading given by a radiation measuring instrument as a function of the value of the quantity to be measured. The important goals of calibrating an instrument are checking whether the instrument is working independent of controlled set of standard conditions and to check whether the instrument is adequate for the intended purpose. Calibration helps to adjust the performance of the instrument thereby overall measurement accuracy of it can be optimized. At present, calibration is carried out by dismantling the instruments and taking them to the calibration facility where calibration is being carried out at least one point on each measuring range of the instrument or in each decade of the reading scale of the instrument in a logarithmic scale. Performance evaluation is done at a radiation field of 50% of the each range/decade of the instrument. The instruments exposed with dose rate above a set value of alarm helps in testing of annunciation of alarms. This procedure results in downtime of the instruments which involves removing and reaffixing of monitors and hence causes interruptions in the uninterrupted radiation field monitoring. Apart from this, contribution of Gamma scattering from back wall and other structures in the calibration facility are also not considered during the calibration of these instruments. To overcome these limitations, an in-situ calibration system for calibration of

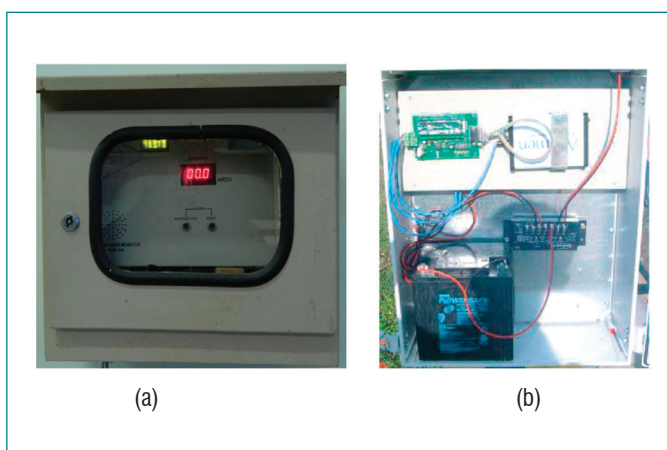


Figure 1: (a) Area Gamma Monitor (b) Autonomous Gamma Dose Loggers

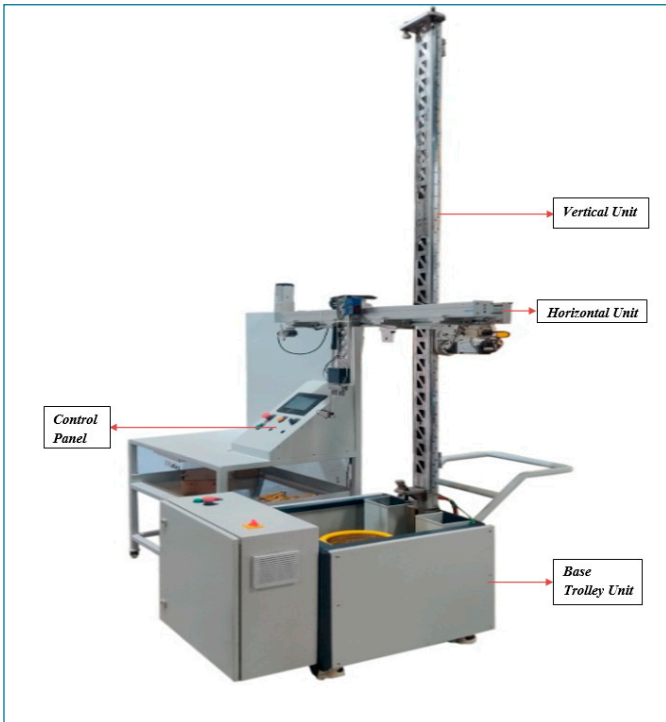


Figure 2: A complete view of in- situ calibrator setup

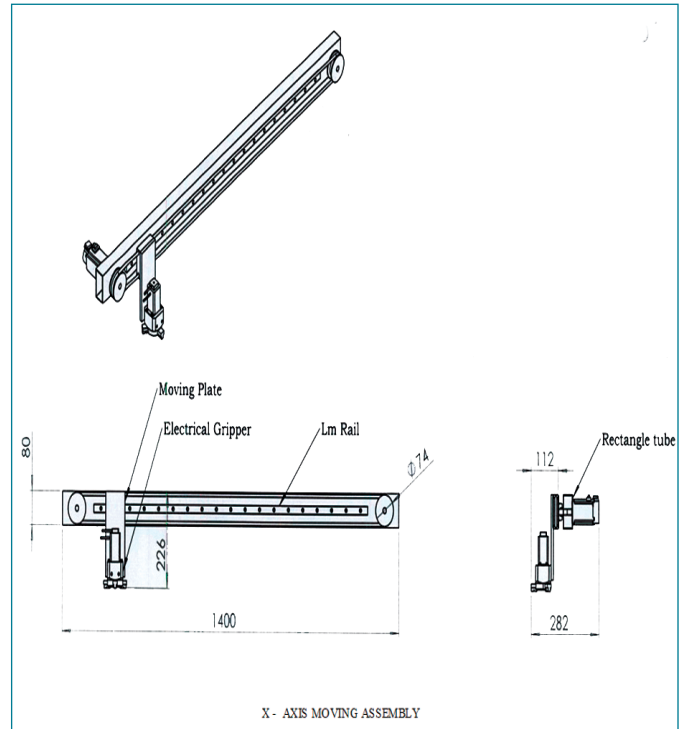


Figure 4: X axis moving assembly along with its top and front view.

AGM and AGDL has been developed. It is a mobile version with fast assembling function integrated with robotic system. For the efficient calibration of these instruments, a clear understanding of the various parameters such as range of the detector, accuracy etc is required.

### Area Gamma Monitors and Autonomous Gamma Dose Loggers

The AGM has generally working range of 0.01 to 100mR/hr or 0.1 to 1mSv/hr and it can be extended to 10R/hr. Energy compensated, halogen-quenched GM tube GM131E is used as a detector in most of the AGMs. These AGMs indicate dose rate digitally on 6x7 segment LED display or 16x2 LCD display. There are two visual annunciator lamp windows, green and red, for normal and active conditions. The active window displays the current dose rate value during normal operating condition and flashes once it exceeds the set dose rate limit. The detection accuracy is  $\pm 10\%$  throughout the range with Caesium source.

AGDL is a microcontroller based system which has a LCD display for the measurement of instantaneous dose rate with date and time

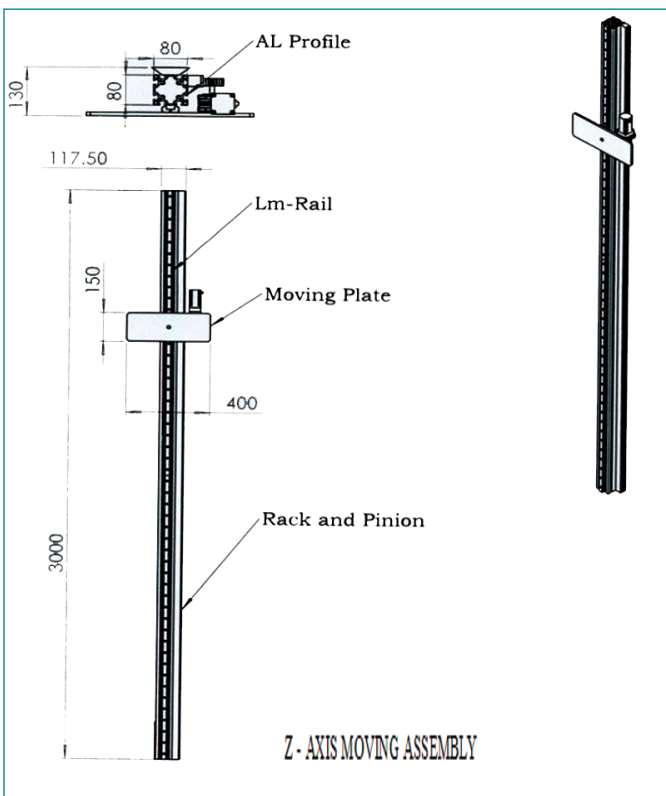


Figure 3: Z Axis moving assembly along with its top and front view

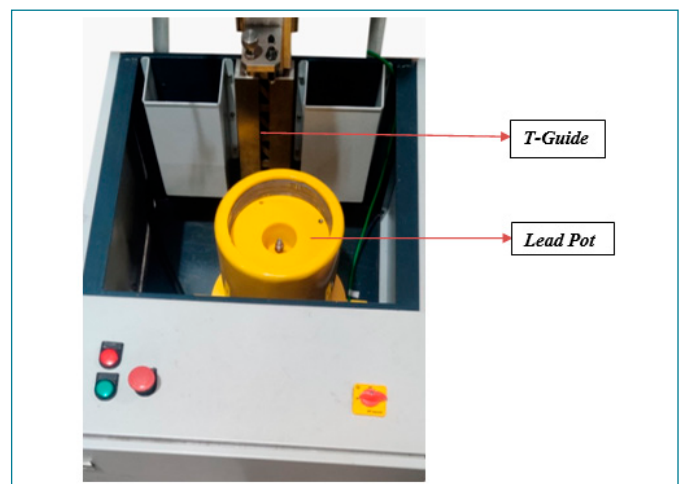


Figure 5: Base trolley containing lead pot, two trays and T-guide

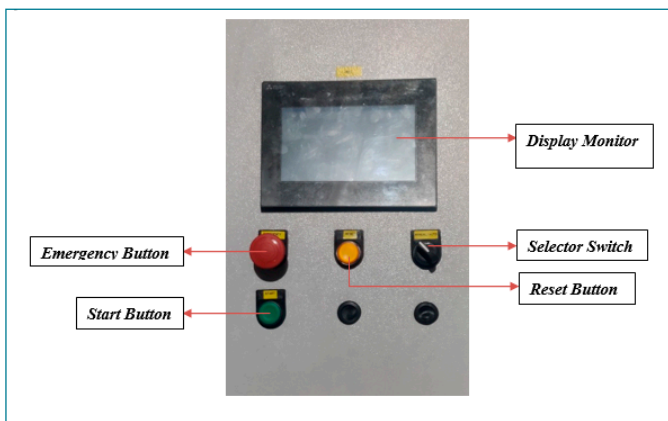


Figure 6: Control panel/ HMI indicating all switches

stamps and standard deviation for the logged data. It continuously monitors and stores environmental gamma dose rate with preset time intervals. It uses two energy compensated Halogen quenched GM tubes (a lower range and a higher range) viz. Centronics make ZP1221 (lower range) and ZP1301 (higher range). The range of measurement varies from 100nGy/hr to 5Gy/hr. AGDL is a standalone environmental monitor which works with the help of solar energy and transfers the measured data as radio frequency signals to data acquisition system. It helps to ensure the continuous background monitoring of radiation level and detects higher dose rate due to excess release and to be used for the estimation of source term for decision making in emergency condition. Figure 1a and 1b shows an AGM and AGDL respectively.

**Salient features of In-situ Calibration System**

In-situ calibration system is a complete automated system which ascertains the effective functioning of AGMs and AGDLs mounted at different places with varying heights. The in-situ calibration system has mainly four components namely vertical unit, horizontal unit, base trolley with lead pot storage, and electrical unit. A typical photograph of the in-situ calibration system is given in Figure 2.

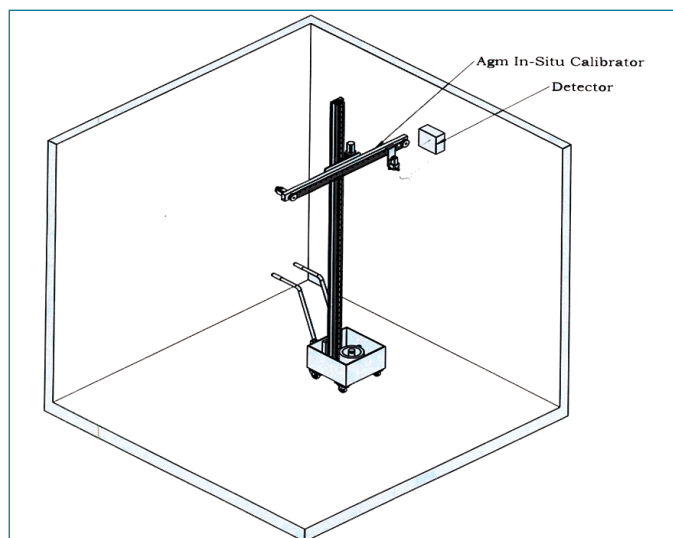


Figure 7: In situ calibrator setup aligned with detector

**Vertical Unit**

Vertical unit provides the complete vertical motion of the system which consists of vertical support setup included with Z-axis Linear Motion rail and block assembly, Z-rack and pinion setup, moving plate assembly, locking setup for movement, servo motor with drive, limit switches and shock absorber. Vertical system has a height of 3025mm from the base of Chamber Box and Z axis travel length of 3000mm. Vertical support setup provides complete support to the entire overhung horizontal unit which is made of aluminium profile channel. Choice of aluminium material is due to interaction with gamma and its light weight nature has the potential to increase the portability. Linear Motion(LM) rails has a profiled rail and a bearing block which provides a linear motion by re-circulating rolling elements. This LM rail establishes high precision and enhanced accuracy in the movement operation. Z-rack and pinion setup of LM rail provides slip free and better controlled motion for the moving plate. The complete setup for Z axis motion (Z axis moving assembly) and its top view, front view is shown in Figure 3.

**Horizontal Unit**

The horizontal unit consists of horizontal support setup, X-axis linear motion rail and block assembly, moving plate assembly, linear actuator, rotation pivot setup, servo motor with drive and gripper set. But here the motion is facilitated by a simple linear actuator instead of Z-rack and pinion setup because moving plate for horizontal direction has to take the load of the source alone. The complete horizontal setup is shown in Figure 4. The important feature of in-situ calibration system is gripper set which is an electric gripper consisting of an electric motor and gripper fingers. It enables the smooth handling of the source. The motion of gripper fingers can be controlled using electric motor and linear actuators which are made up of aluminium. Hence the proper clamping of source will be done by the customized gripper fingers. Video-1 demonstrating the remote handling of the source during calibration.

**Base Trolley Unit**

The system has trolley setup for smooth mobility of the complete system to the designated place. Trolley has a square base of 450mm side length and swivel moving is possible with castor wheels, which allows movement in all possible directions. There is a custom designed lead pot inside the trolley for the temporary storage of the source during calibration. This lead pot provides sufficient shielding for the source and which is permanently mounted on the base plate of the trolley. There is a T-slot guide mounted inside the trolley for the proper clamping of the vertical support set-up unit. During the assembling, the vertical unit has to be inserted in the T-slot and tightened to makes the vertical unit rigid. The arrangement inside the base trolley is given in Figure 5.

**Electrical Unit**

The user friendly electronics and control unit consists of camera,

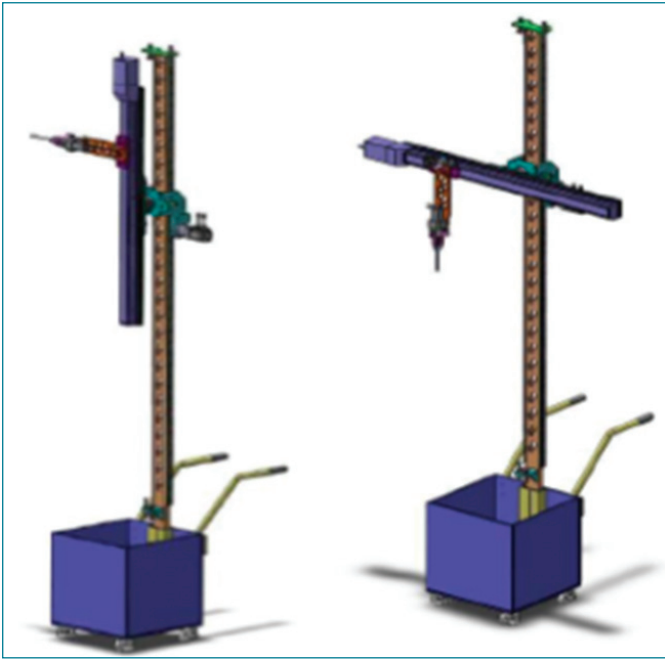


Figure 8: Position of horizontal setup (a) home position and (b) during calibration

control panel, laser sensor, distance sensor, programmable logic controller (PLC), and Human Machine Interface (HMI) programming. Control panel is mounted behind the trolley. Camera is mounted on the horizontal axis to appropriately capture the instantaneous dose rates during the calibration. A camera monitor placed on the operating table shows the captured values during calibration. Electronic/ electrical limit switches are provided for forward and reverse linear movement for safety. A distance sensor is facilitating the stoppage of source at multiple positions on the horizontal axis given by the user. Laser sensor is employed for the proper alignment of detector and source. The Control panel consists of switches for various operations like Start, Stop, Manual, Auto etc. In case of emergency the full system can be safely shutdown by pressing the Emergency button and a reset button will help the system to come back to its normal position. A display on the control panel shows the mode of operation, X-axis distances, etc. A typical picture of control panel with its switches is shown in Figure 6. The secure operation of whole system is achieved using password protection. This operating system (control panel) can be operated at a distance of 10m and it is useful in reducing personal exposure to large extent. Speed of all movements can be controllable using HMI and have a complete PLC based operating station. Each movement of the axis will be in close loop system so that feedback of the intermediate position can be monitored. PLC and HMI helps to avoid close interaction of human with source loaded calibrator system during calibration. These data will be stored on the hard disc of the system which can be accessed later for evaluation through USB ports.

#### System Operation

The system is brought to the proximity of the AGM/AGDL system

#### Video 1: Remote handling of source during calibration

using trolley arrangement. The alignment of the source with detector is carried out manually by using the provided laser sensor to fix the detector and source in a straight-line position and as close as possible, because, the detector of AGM/ AGDL is encapsulated in a cover (body of the system). The manual mode operation is performed to register the height of the detector without the upbringing of source and various source-detector distances are ascertained. The X-axis increments have to be given as input in steps of 1cm to 100cm on HMI for measurement at desired points. Then the system is operated in an automated mode along with source gripped during the calibration and varying horizontal distances. The calibration of the AGM and AGDL is carried out with two commonly and widely used gamma sources Co-60 and Cs-137. Co-60 has half-life of 5.27 years and it has two gamma rays of energy 1.17MeV and 1.33MeV each with emission probability of 100%. Cs-137 produces gamma rays with energies of 0.662MeV and has a longer half-life of 30.1years. Here Co-60 source of appropriate activity is used in the calibrator for the calibration process. The dose rate at the detector position at each calibration point is determined by placing the calibrated Ionisation Chamber(IC) at detector location. After the establishment of the true dose rate value at various calibration points for that particular AGM/ AGDL, the data can be used for adjustment of optimized operation of the AGM/AGDL and for periodic recalibration. The entire assembled in-situ calibration system aligned with detector is shown in Figure 7. After successful completion of the calibration process the gripper returns to its home position and horizontal unit moves down and drop the source inside the lead pot. Then horizontal unit moves back to its home position and then lead pot is closed. The X-axis can be brought to be in line with Z-axis and dismantling it from the trolley can be initiated. The two different positions of Horizontal unit at resting position (home position) (a) and during operation (b) are shown in Figure 8.

In future it is proposed to make the control panel as a handheld system like a cell phone to increase its portability and make it more user friendly. Thus, this system is designed to minimise the radiation exposure to the operator and down time of the AGM and AGDL during the calibration process.

## Young Researcher's Forum



Ms. Manali Nandy is working as a young research scholar in SMARTS, MCG. After acquiring M. Sc. in Physics from Lady Brabourne College, University of Calcutta, she joined IGCAR in 2016 as junior research fellow. She registered for PhD in HBNI under the guidance of Dr. John Philip. Her thesis is titled as "Magnetic nanoemulsion based sensors for visual detection of defects in ferromagnetic materials: Effect of stabilizing moieties and defect geometries on the detection sensitivity". She has authored 06 journal publications, attended 05 conferences and received the Young Scientist Award (winner), 2021 by Dr. K. V. Rao Scientific Society, India. She is currently pursuing a post doctoral research at Wageningen University, Netherland.

# Inter-droplet Force Between Magnetically Polarizable Pickering Oil-in-water Nanoemulsions Stabilized with $\gamma$ -Al<sub>2</sub>O<sub>3</sub> Nanoparticles: Role of Electrostatic and Electric Dipolar Interactions

Emulsions are binary mixtures of two immiscible liquids that are thermodynamically unstable but kinetic stability is imparted by designing the interphase with various types of moieties, like surfactants, polymers, polyelectrolytes, nanoparticles, etc. Emulsions are abundantly used in diverse industries like food, beverages, pharmaceuticals, cosmetics, detergents, paints, etc. Hence, longer shelf-life and superior colloidal stability with negligible degradation with ageing are the most desirable properties of such emulsions, especially for industrial applications.

Classical emulsions, stabilized by using surfactants or polymers are well studied over a long period of time. Of late, it has been demonstrated that nanoparticle stabilized emulsions or Pickering emulsions exhibit significantly better colloidal stability, as compared to classical emulsions, due to stronger adsorption of the nanoparticles at the oil water interface. In the case of adsorption of 10 nm sized  $\gamma$ -Al<sub>2</sub>O<sub>3</sub> nanoparticles at octane-water interface, the adsorption energy is found to be  $\sim 10^3 k_B T$ , whereas for short chain length surfactants, the adsorption energy is  $\sim k_B T$ , which has inspired a broad range of research in this area. The stabilization mechanism of the Pickering emulsion is primarily dictated by the three phase contact angle of the nanoparticles in aqueous medium and a value close to 90° has been found to be the most beneficial. Also, the size of the nanoparticle is required to be an order of magnitude smaller than the emulsion droplets for a compact coverage of the oil-water interface, which is essential for enhancing the colloidal stability.

The preparation and stabilization of functional Pickering emulsions for varied applications have been studied earlier. Such nanoparticle stabilized Pickering emulsions have found applications in the field of enhanced oil recovery, drug delivery, magnetic hyperthermia, etc., where the conditional stabilization-destabilization of the emulsion is highly beneficial, which can be effectively achieved by tuning the physio-chemical nature of the interfacially adsorbed nanoparticles. Though the steric or Coulombic stabilization of classical surfactant or polymer stabilized emulsions is well understood, proper investigation on the nature of colloidal forces between interacting Pickering nanoemulsion droplets under the influence of varying physio-chemical properties is still scarce. The scenario becomes further complicated in the case of charged particle stabilized Pickering emulsions, as the nanoparticles are adsorbed strongly at the oil-water interface, rendering static charges at the interface over timescales significantly larger than the dynamic charges in the case of anionic or cationic surfactant stabilized classical emulsions.

With this objective, here, at Indira Gandhi Centre for Atomic Research, we have aimed at measuring the colloidal force between interacting  $\gamma$ -Al<sub>2</sub>O<sub>3</sub> nanoparticle stabilized Pickering nanoemulsion droplets, at varied pH and salt concentrations, utilizing an in-house developed magnetic chaining based force spectroscopy technique, which is capable of measuring weak ( $\sim 10^{-14}$  N) colloidal forces. In this study, for the first time, the effect of electric dipolar interaction on the colloidal force between interacting charged

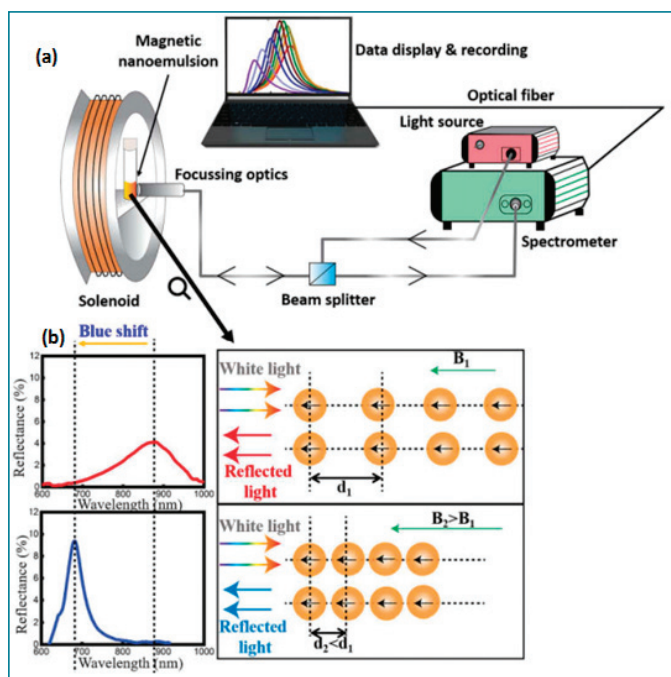


Figure 1: (a) Schematic representation of magnetic chaining technique. (b) The blue-shift of Bragg peak corresponding to decrement in inter droplet separation with increasing magnetic field.

particle stabilized Pickering nanoemulsion is probed experimentally and theoretically over a wide pH range and salt concentrations. The obtained results offer better understanding on the nature of colloidal interaction, which is essential for preparation of Pickering emulsions for varied applications.

To prepare colloiddally stable Pickering magnetic nanoemulsion utilizing  $\gamma$ - $\text{Al}_2\text{O}_3$  nanoparticles as stabilizers, a low energy emulsification technique is utilized. The size, three phase contact angle, solution pH and concentration of the nanoparticles were systematically optimized for ensuring compact coverage of the oil-water interface, which is essential for colloidal stability. At first, crude polydisperse SDS stabilized ferrofluid emulsion was prepared by shearing SDS solution, octane based ferrofluid and water at room temperature in the mass ratio of 5:90:5. Following this step, the magnetic nanoemulsion was made monodisperse (average hydrodynamic diameter  $\sim 200$  nm with a poly dispersity index of 0.06) by employing sequential fractionation technique. Thereafter,  $\gamma$ - $\text{Al}_2\text{O}_3$  nanoparticle stabilized Pickering nanoemulsion of average hydrodynamic diameter  $\sim 253$  nm was prepared by solution exchange route, where the solution pH was optimized to facilitate adsorption of the charged nanoparticles at the oil-water interface.

Colloidal force measurements were performed using an in-house developed magnetic chaining technique, comprising of a solenoid type electromagnet, programmable current source, tungsten-halogen white light source and a fiber-optic spectrometer. In this technique, the repulsive inter-droplet force magnitude were recorded as a function of inter-droplet spacing, which is expressed as  $d-2r_e$ ,

where,  $d$  and  $r_e$  indicate the centre-to-centre distance between two neighbouring nanoemulsion droplets and hydrodynamic radius of an emulsion droplet, respectively. Fig. 1a schematically shows the experimental set-up. The magnetic nanoemulsion droplets undergo Brownian motion in the absence of an external magnetic field, whereas in the presence of a magnetic field, they form one dimensional ordered linear chain-like structures in the direction of the magnetic field induced by magnetic dipolar interaction. As the ordered chain-like structures are illuminated by white light in the direction parallel to the magnetic field, Bragg reflection is observed in the  $180^\circ$  backscattered direction when the inter-droplet spacing matches with the wavelength of incident light, and the Bragg condition is satisfied:  $d = \lambda_{\text{max}} / 2\eta$ , where,  $\lambda_{\text{max}}$  and  $\eta$  indicate the Bragg peak wavelength and refractive index of the medium, respectively. With increasing magnetic field, the induced magnetic moment of the emulsion droplets increases, leading to a smaller inter-droplet separation, which causes a reduction in the Bragg reflected peak wavelength. Hence, with increasing magnetic field, the Bragg peaks are blue shifted. The phenomenon is schematically shown in the Fig. 1b.

In the presence of magnetic field, the formation of linear chain-like structures, consisting of the nanoemulsion droplets, occurs when the magnetic attractive force balances the repulsive force. The formation of liner chain-like structures was experimentally confirmed using atomic force microscopy technique. Fig. 2a shows the typical  $90 \mu\text{m} \times 90 \mu\text{m}$  atomic force microscopy topographic image of the  $\gamma$ - $\text{Al}_2\text{O}_3$  nanoparticle stabilized Pickering nanoemulsion, dried in-situ on a mica substrate, in the presence

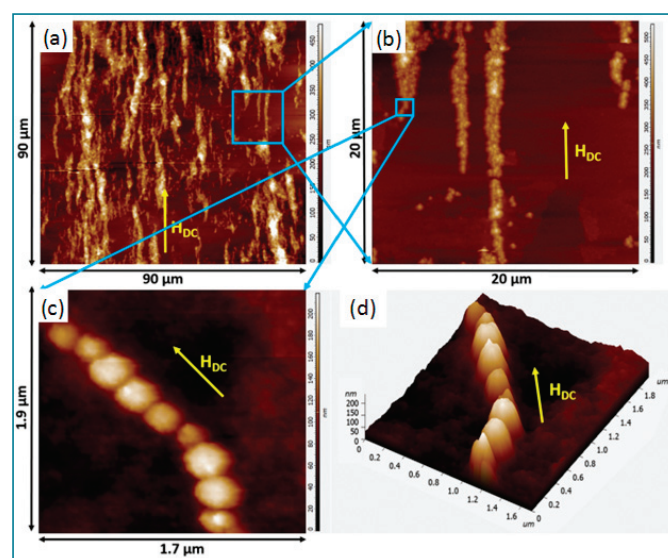


Figure 2: (a) Typical  $90 \mu\text{m} \times 90 \mu\text{m}$  atomic force topography image of the  $\gamma$ - $\text{Al}_2\text{O}_3$  stabilized magnetic nanoemulsion, under the presence of an external magnetic field  $\sim 250$  G (indicated by an arrow in the figure). (b)  $20 \mu\text{m} \times 20 \mu\text{m}$  magnified topographic view of a section of (a), as indicated by the blue rectangle. (c)  $1.7 \mu\text{m} \times 1.9 \mu\text{m}$  magnified topography image of a section of (b). (d) Three-dimensional topography image corresponding to (c).

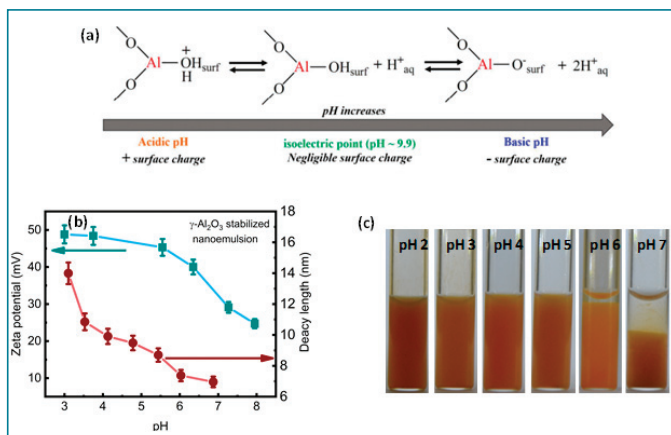


Figure 3: (a) Alteration of  $-Al-OH$  surface group with varying pH. (b) Variation of zeta potential and decay length of force of  $\gamma-Al_2O_3$  stabilized nanoemulsion with increasing pH. (c) Digital Pictures of stabilized magnetic nanoemulsion with increasing pH, where destabilization is initiated around pH  $\sim 7$ .

of an external magnetic field  $\sim 250$  G. Fig. 2b shows a typical  $20 \mu m \times 20 \mu m$  magnified topographic image of a section of Fig. 2a, where several bundles of linear chains, oriented parallel to the direction of the magnetic field, are clearly seen. Fig. 2c shows the  $1.7 \mu m \times 1.9 \mu m$  magnified topography image of a section of Fig. 2b, where, a single chain of individual nanoemulsion droplets is observed. Fig. 2d shows the corresponding three dimensional topographic image, where the typical topographic height of the nanoemulsion droplets was found to be  $\sim 235 \pm 40$  nm, which was in agreement with the data obtained from hydrodynamic diameter measurements.

The repulsive forces are being supplied by the surface-active moieties stabilizing the magnetic nanoemulsion ( $\gamma-Al_2O_3$ ) nanoparticles, in this case). On the other hand, the attractive forces are due to magnetic dipolar forces ( $F_{mag}$ ) and van der Waals forces ( $F_{vdw}$ ). The magnetic dipolar force for chains is expressed as  $F_{m,d} = \sum_{i=1}^s \sum_{j=1}^m \frac{6m_i m_j}{(d_{ij})^3} - \zeta(3) \frac{6m^2}{d^3}$ , where,  $s$  indicates the number of droplets in the chain and  $m$  is the magnetic dipole moment, which is expressed as:  $m = \frac{4\pi r^3 \chi_f H_T}{3}$ , where  $\chi_f$  and  $H_T$  denote the ferrofluid susceptibility and total magnetic field (i.e., applied and induced), respectively, and  $\zeta(3) = 1.202$ . The van der Waals force was found negligible in the present case and hence, neglected.

In order to prove the high colloidal stability of the  $\gamma-Al_2O_3$  stabilized magnetic nanoemulsion, the estimation of adsorption free energy of nanoparticles at the oil-water interface is essential. The Gibbs free energy ( $\Delta G_{ads}$ ) of spherical nanoparticle adsorbed at a flat oil-water interface is expressed as:  $\Delta G_{ads} = \pi r^2 \gamma_{ow} (1 - |\cos \theta_w|)^2$ , where  $\gamma_{ow}$  and  $\theta_w$  indicate the oil-water interfacial tension and three phase contact angle of the nanoparticle situated at the oil-water interface, respectively. In the present case, for octane-water interface,  $\gamma_{ow} = 50$  mNm $^{-1}$  and  $\theta_w \sim 76^\circ \pm 4$ , which resulted in  $\Delta G_{ads} \approx 0.8 \times 10^3$  k $_B$ T, i.e., the adsorption energy is found to

be  $\sim 10^3$  times higher than the thermal energy, which indicated the strong adsorption of the  $\gamma-Al_2O_3$  nanoparticles at the oil-water interface, thereby enhancing the colloidal stability of the  $\gamma-Al_2O_3$  nanoparticle stabilized Pickering nanoemulsions.

The  $\gamma-Al_2O_3$  nanoparticles display amphoteric behaviour in aqueous solution because of the formation of  $-Al-OH$  group at the nanoparticle surface and exhibit zeta potential  $\sim 55$  mV at pH 3. The iso-electric point of  $\gamma-Al_2O_3$  nanoparticles was found to be at pH  $\sim 9.9$  which signified that below this pH, the surface charge turned positive due to progressive transformation of  $-Al-OH$  group to  $-Al-OH_2^+$  and above this pH, the surface charge turned gradually negative aided by progressive transformation of  $-Al-OH$  group to  $-Al-O^-$  as shown in Fig. 3a. The gradual change in surface charge was reflected in the zeta potential measurement of  $\gamma-Al_2O_3$  stabilized magnetic nanoemulsion with pH as shown in Fig. 3b. As the pH tended towards iso-electric point, the zeta potential decreased from  $\sim 49 \pm 3$  mV to  $\sim 24.7 \pm 3.6$  mV on increasing the pH from  $\sim 3.1$  to  $\sim 8$ . Alongside, the regression analyses were carried out on the experimentally obtained force profiles by the exponential decay function  $F(d-2r_c) = F_m \exp\left[-\frac{(d-2r_c)}{\lambda_d}\right]$ , where,  $F_m$  and  $\lambda_d$  represent the force magnitude and decay length of force. Fig. 3b also displays the decrement of decay length of the interaction forces with increasing pH. It can further be observed that the decay length of the Pickering nanoemulsion decreased from  $14 \pm 1$  nm to  $6.9 \pm 1.5$  nm ( $\sim 51\%$ ) for nearly 2.3-fold increase in pH. Fig. 3c depicts the digital pictures of  $\gamma-Al_2O_3$  nanoparticle stabilized magnetic nanoemulsions at different pH, where complete phase separation was observed at pH  $\sim 7$ . As the pH value of the  $\gamma-Al_2O_3$  nanoparticle stabilized magnetic emulsion increased, the nanoemulsion exhibited sudden destabilization at pH  $\sim 7$  owing to the increased agglomeration of the nanoemulsion droplets induced by pH-dependent reduction of electrostatic repulsion between the droplets. This phenomenon clearly shows the potential application of  $\gamma-Al_2O_3$  stabilized magnetic nanoemulsion in the field of enhanced oil recovery and drug delivery where the conditional (pH-dependent) destabilization would prove beneficial.

The positively charged  $\gamma-Al_2O_3$  nanoparticles give rise to electric double layer in aqueous medium. In the case of thin double layer ( $\kappa r_c > 5$ ), Derjaguin approximation provides the theoretical expression of electrostatic repulsion as  $F_e(d) = 2\pi\epsilon\psi_0^2 r_c^2 \frac{\exp[-\kappa(d-2r_c)]}{1 + \exp[-\kappa(d-2r_c)]}$ , where,  $\kappa$ ,  $\epsilon$  and  $\psi_0$  indicate the inverse of the electrostatic Debye length, dielectric constant of medium and surface potential, respectively. In order to probe the effect of ionic strength on the force profiles of  $\gamma-Al_2O_3$  stabilized magnetic nanoemulsion, the effects of progressive increment of monovalent (NaCl), divalent (CaCl $_2$ ) and trivalent (Fe $_2$ (SO $_4$ ) $_3$ ) salts were investigated at pH  $\sim 3.1$ . The theoretical Debye length ( $\lambda_D$ ) is calculated by  $\lambda_D = \kappa^{-1} = \left[ \frac{\epsilon_0 \epsilon_r}{\sum C_i z_i^2} \right]^{1/2}$ , where,  $i$ ,  $z_i$ ,  $C_i$ ,  $C_{0i}$ ,  $\epsilon_0$  and  $e$  represent the valence of ions species  $i$ , ionic molar concentration of species  $i$ , bulk concentration of ions species

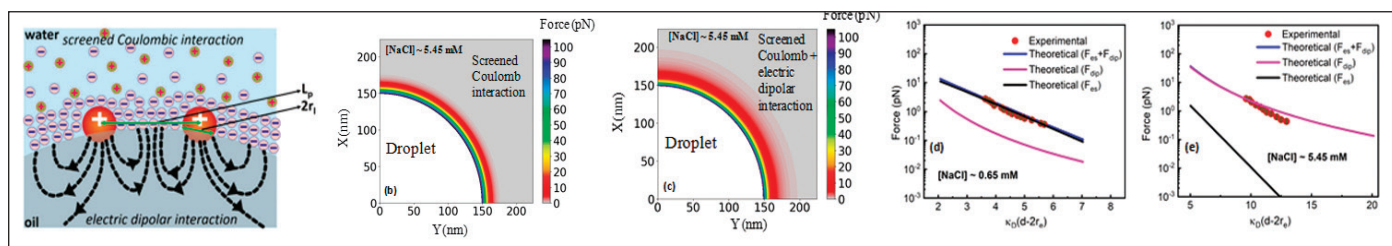


Figure 4: (a) Schematic representation of the oil–water interface decorated with positively charged  $\gamma\text{-Al}_2\text{O}_3$  nanoparticles. Surface plots showing the theoretically calculated repulsive force magnitudes around a single nanoemulsion droplet in 1st quadrant, for the (b) screened Coulombic interaction alone and (c) screened Coulombic interaction along with electric dipolar interaction. Variations of inter-droplet force magnitudes (experimental and theoretical values calculated with and without incorporating the electric dipolar interaction), as a function of normalized distance,  $\kappa D(d-2r_e)$  for (d) 0.65 mM NaCl and (e) 5.45 mM NaCl.

$\epsilon_0$ , permittivity of free space and electron charge, respectively. The decay lengths ( $\lambda_d$ ) obtained from the regression analysis of force measurement and the theoretical Debye length ( $\lambda_D$ ) were compared for the varied concentrations of mono-, di- and trivalent salts, and it was found that the theoretical values were systematically lower than the experimental decay lengths in all cases. Regression analyses revealed that the experimental decay lengths varied as  $\lambda_d = [\text{Na}^+]^{-0.24 \pm 0.01}$ ,  $\lambda_d = [\text{Ca}^{2+}]^{-0.25 \pm 0.01}$  and  $\lambda_d = [\text{Fe}^{3+}]^{-0.27 \pm 0.01}$  for mono-, di- and trivalent salt concentrations, respectively. This also indicated deviations from the classical Debye-Huckel model, which required further investigations.

The charged nanoparticles situated at the oil-water interface gives rise to electric dipoles perpendicular to the interface due to the formation of asymmetric charge cloud of the counter-ions. In the aqueous medium, the fixed charges generated screened Coulombic interaction owing to the presence of co-ions and counter-ions, whereas in the non-polar medium, the charges generated electric dipolar interaction, which showed long-range asymptotic behaviour. Fig. 4a schematically depicts an oil-water interface decorated with positively charged  $\gamma\text{-Al}_2\text{O}_3$  nanoparticles, which gives rise to screened Coulombic interaction in the aqueous phase and electric dipolar interaction in the oil phase. The electric dipolar interaction ( $F_{\text{dip}}$ ) is expressed as:  $F_{\text{dip}} = \frac{3p_{\text{dip}}^2}{2\epsilon_0 L_p^4}$ , which is valid for  $L_p > r_1$ , neglecting the electro-capillary force due to higher Laplace pressure of smaller sized nanoemulsion droplet. Here  $L_p$  and  $r_1$  indicate the separation between two approaching  $\gamma\text{-Al}_2\text{O}_3$  nanoparticles and contact line radius, respectively. The dipole moment ( $p_{\text{dip}}$ ) is expressed as:  $p_{\text{dip}} = \frac{2\epsilon_0 q_{\text{surf}}}{\epsilon_w \kappa}$ , where  $\epsilon_w$  and  $\kappa$  denote the dielectric constant of water and theoretical inverse of Debye length. The total surface charge ( $q_{\text{surf}}$ ) is calculated by  $q_{\text{surf}} = 4\pi\sigma_{\text{surf}}r_p^2$ , where the surface charge density is expressed as:  $\sigma_{\text{surf}} = \sqrt{8\epsilon_0 k_B T C_{\text{el}} \sinh\left(\frac{z\psi_0}{2k_B T}\right)}$ . Here,  $\psi_0$  indicates the surface potential, which is approximated as the zeta potential in the present case. Incorporating the electric dipolar interaction, in addition to the screened Coulombic interaction, the expression for the total inter-droplet force profiles was:  $F_{\text{tot}} = F_{\text{es}} + F_{\text{dip}} = 2\pi\epsilon_0 \psi_0^2 r_p \kappa \frac{\exp[-\kappa(d-2r_e)]}{1 + \exp[-\kappa(d-2r_e)]} + \frac{3p_{\text{dip}}^2}{2\epsilon_0 L_p^4}$ , which was used for theoretical calculations.

Using the above mentioned force equation, the surface plots of the total interaction forces were theoretically simulated around a single nanoemulsion droplet in 1<sup>st</sup> quadrant for NaCl concentration of  $\sim 5.45$  mM. Fig. 4b shows the surface plot of screened Coulomb interaction only, whereas, Fig. 4c depicts the surface plot of total force (both screened Coulomb and electric dipolar interaction), which displays significantly extended interaction length upon incorporation of electric dipolar interaction.

The theoretically calculated total force ( $F_{\text{tot}}$ ),  $F_{\text{es}}$  and  $F_{\text{dip}}$  along with the experimental data for NaCl concentrations of 0.65 mM and 5.45 mM are shown in Fig. 4d and 4e, respectively. Comparative analysis shows that the experimental data were in good agreement with total force  $F_{\text{tot}}$  after inclusion of the electric dipolar interaction, especially at higher salt concentration. It was further observed that the screened Coulombic interaction contributed more at lower salt concentration. However, the electric dipolar interaction turned out to be the primary contributor in the case of higher salt concentration. Similar results were obtained for the di- and trivalent salts of varied concentrations, which showed that the screened Coulomb interaction was major contributor in the total repulsive force at lower salt concentrations, whereas, electric dipolar interaction was the primary contributor at higher salt concentration.

Our experimental results and theoretical calculations, for the first time, showed the importance of electric dipolar interaction on the colloidal force between interacting charged particle stabilized Pickering nanoemulsion droplets. The insights obtained on the nature of colloidal interaction forces is immensely beneficial for preparation and stabilization of Pickering nanoemulsions with enhanced colloidal stability and shelf-life. The unique insight about the inter-droplet force in the Pickering emulsion is a useful tool for further tuning the stability of Pickering emulsions using the stimuli-responsive behaviour of the stabilizing nanoparticles, which finds applications in enhanced oil recovery, drug delivery and magnetic fluid hyperthermia based cancer therapy in near future.

## All India Hindi Scientific Seminar Role of Nuclear and other Advanced Technologies for Climate Change Control

January 10-11, 2023



### Glimpses of the All India Hindi Scientific Seminar-2023

On the occasion of World Hindi Day (January 10), An All India Hindi Scientific Seminar was organized by the Official Language Implementation Committee of Indira Gandhi Atomic Research Centre, Kalpakkam jointly with Bhartiya NabhiyaVidyut Nigam Limited, Kalpakkam and General Services Organisation, Kalpakkam at Sarabhai Auditorium, Homi Bhabha Bhavan, IGCAR on January 10 and 11, 2023. The title of the seminar was “Role of Nuclear and other Advanced Technologies for Climate Change Control”. Dr. G.K. Dey, Former Director, Materials Division, BARC was present as a chief guest of the inaugural function of the seminar. Dr. B. Venkataraman, Director, IGCAR presided over the seminar. Addressing the audience, he said that keeping in mind the environment protection, the Department of Atomic Energy is

committed to the development of green energy production and climate-friendly innovative technologies. Scientific and technical officers and research scholars from the units of the Department of Atomic Energy, major scientific and research institutes, public sector establishments, all India educational institutions located across the country registered their participation in the seminar. A total number of 6 technical sessions were organized during the seminar, in which 13 invited talks, 14 contributory talks and 47 posters were presented. A total of 85 general participants were present in the seminar.

*Reported by  
Prabhat Kumar Sharma, DD (OL)*

## Hindi Workshop

February 02, 2023



### Glimpses of Hindi Workshop

A one day Hindi workshop was organized on 16-02-2023 at Raja Ramanna Auditorium for the employees of IGCAR, Kalpakkam during January-March quarter. The workshop was divided into a total of four sessions. In the first session, Shri Raju Pandey, Sr. Manager (Official Language), BHAVINI, Kalpakkam delivered his lecture on the topic of Official Language Policy. In the second session, the employees were made to practice noting and drafting in Hindi by Shri Sunil Kumar Jangid, Hindi teacher, Hindi Teaching Scheme. In the third session which started after lunch, Shri Prabhat Kumar Sharma, Deputy Director (Official Language), Hindi

Section, IGCAR delivered his lecture on Hindi Incentive Scheme of DAE (ATOLIS) and encouraged them to participate in that scheme. In the fourth and last session, employees participating in the workshop were given information about the use of Hindi on computer and were given Hindi typing practice by Shri Jitendra Gupta, UDC, Hindi Section, IGCAR. The workshop ended with a feedback and valedictory session followed by tea.

*Reported by  
Prabhat Kumar Sharma, DD (OL)*

## Report on Transfer of IGCAR's Conductivity Meter Technology

March - 17, 2023.



Transfer of IGCAR's Pulsating Sensor based Conductivity Meter technology to a Mumbai based industry on 17.March.2023. This event was organized by TT&CD, BARC, Mumbai.

IGCAR's "Pulsating Sensor based Conductivity Meter" technology, developed in the Electronics and Instrumentation Group to meet India's Atma Nirbhar Bharat goals was transferred to a Mumbai private industry on March 17, 2023. In a brief event arranged by Technology Transfer & Collaborations Division, BARC, the technology license agreement was exchanged between the Director of the private industry and Dr. A. P. Tiwari (Director, Knowledge Management Group, BARC & Chairman, Technology Transfer Sub-Committee of DAE). Dr. N. Subramanian, Head, Incubation Centre-IGCAR handed over the Technology Document to the

industry. The meeting was attended by Dr. Amar Banerji, Head, TT & CD, BARC and his senior colleagues, Shri M. Sivaramakrishna, Head, ISS, EIG, IGCAR and Directors of the Mumbai licensee. This is the third industry to which this technology has been transferred to on a non-exclusive basis since April 2021.

*Reported by  
Dr. N. Subramanian  
Safety, Quality & Resource Management Group*

## Women's Day Celebrations at IGCAR 2023

March 1- 7, 2023



Felicitation to school children

Women's Day was celebrated from March 1- 7, 2023, at IGCAR. The celebrations included competitions and felicitating girl students who have excelled in studies, sports and cultural events. Distinguished women in law and justice, news broadcasting and financial advice were invited to share their experiences and educate the audience.

Ministry of Women and Child Development had directed DAE

to create awareness about the schemes developed by the government for the welfare of women and to felicitate achievement by women during the week of March 1 to March 8 through various celebrations.

IGCAR organized competitions like slogan writing, posters, elocution and skits on topics related to Women's empowerment. Such competitions are the best method to spread the concept



Felicitation to Mehetva founder member Mrs Blossom Rodriguez,



International Women's day celebrations

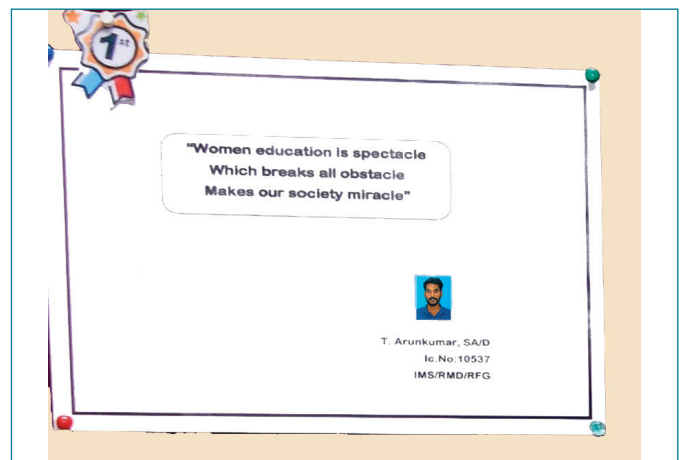
and the various schemes for women's empowerment. More than 150 employees participated in the competitions. Forty employees played six skits on topics including Women's empowerment, Gender Equality, the Role of working women in society, The benefit of treating women with dignity, Innovative methods to protect women and Government schemes for women. The best slogan is portrayed on the Figure-1.

Ms. Leela Meenakshi IIS, Joint Director, All India Radio, spoke on her experiences in the News services field on March 3, 2023. Ms Renu Maheswari, SEBI registered investment advisor and co-founder Finscholarz Wealth Managers, spoke on "Know Your Money" on March 6, 2023. IWSA organized this lecture.

IGCAR organized an awareness lecture by Ms. Sulekha Beevi, Member Judicial Customs Excise and Service Tax Appellate Tribunal, Chennai Region, on March 7, 2023. The cases between Bajaj & Gill, the Vishakha case, etc., were discussed in this lecture. During the interactive session, the speaker explained the law to protect women against sexual harassment in the workplace.



Felicitating Sri Raghupathy , Director, RDTG,EIG and RFG



First prize - Slogan Competition

As a token of appreciation, a memento was gifted to all women employees of IGCAR and CISF at Kalpakkam on Women's day.

Mehetva is a school at Kalpakkam township where training is given to special children was founded by three women in 1996 and has been run successfully by them since then. The school requires specialized training for teachers and other staff to handle the children. On Women's day celebrations 2023, IGCAR honored the founding members of Mehetva, Ms.Blossom

Rodriguez and present organizing member Ms. Chitra.

A total of 50 students from the neighbouring schools AECS1, AECS2, AECS Anupuram, KV1, KV2 and two Tamil Medium schools from Sadras and Pudupattinam were honored.

*Reported by  
Ms. S. Rajeswari*

*Safety, Quality & Resource Management Group*

## Awards, Honours and Recognitions

**Dr. John Philip** has been selected as an Editorial Board Member of Journal of Magnetism and Magnetic Materials of Elsevier Publishers.

**Dr. Arup Dasgupta** received Fellow of Indian Institute of Metals (IIM) for the year 2022.

**Dr. R. Mythili** received Fellow of Electron Microscopy of Society of India (EMSI) Award for the year 2022 under Materials Science category.

**Dr. Harish Chandra Dey**, received "Welding Science & Technology Award" from IIW-India, Chennai Branch.

## Best Paper/Poster Award

**Ms. B.R. Vaishnavi Krupa** received EMSI-2023 conference – Best poster consolation prize.

**Dr. Arup Dasgupta** received "The above and beyond appreciation for Editorial Leadership" in 2022 from Springer.

**Shri Shailesh Joshi, Ms. Madhusmita Panda, Dr. O. Annalaskhmi, C. Dr. Venkata Srinivas and B. Venkatraman** received the second prize in the best poster award at the 6<sup>th</sup> Asian and Oceanic Congress on Radiation Protection (AOCRP6) international conference held at Mumbai during February 7-11, 2023 for the paper titled "Uranium based Metal Organic Framework as OSL Dosimeter".

## Bio-diversity @ DAE Campus, Kalpakkam

Yellow-billed Babbler



**Yellow-billed Babbler**, formerly known as White headed babblers. It is similar in size like myna. Both male and female look similar in appearance. It has creamy white around eyes, forehead and crown. It has pale bluish white iris, pale green wings and lump.

Editorial Committee Members: Ms. S. Rajeswari, Shri P. Vijaya Gopal, Dr. John Philip, Dr. T. R. Ravindran, Dr. C. V. S. Brahmananda Rao, Shri A. Suriyanarayanan, Shri M. S. Bhagat, Shri G. Venkat Kishore, Ms. Sujatha P.N, Shri M. Rajendra Kumar, Shri S. Kishore, Shri Biswanath Sen, Dr. N. Desigan, Shri Gaddam Pentaiah and Shri K. Varathan